Research article

The effect of an exogenous alternating magnetic field on neural coding in deep spiking neural networks

Lei Guo[1,2,*], Wei Zhang[1,2], Jialei Zhang[1,2]

[1] *State Key Laboratory for Reliability and Intelligence of Electrical Equipment, Hebei University of Technology, Tianjin 300130, P.R. China*
[2] *Key Laboratory of Electromagnetic Field and Electrical Apparatus Reliability of Hebei Province, Hebei University of Technology, Tianjin 300130, P.R. China*

***Correspondence**: 2004008@hebut.edu.cn (Lei Guo)

https://doi.org/10.31083/JIN-170046

Abstract

A ten-layer feed forward network was constructed in the presence of an exogenous alternating magnetic field. Results indicate that for rate coding, the firing rate is increased in the presence of an exogenous alternating magnetic field and particularly with increasing enhancement of the alternating magnetic field amplitude. For temporal coding, in the presence of alternating magnetic field, the interspike intervals of the spiking sequence are decreased and the distribution of interspike intervals tends to be uniform.

Keywords

Spiking neural network; neural coding; reduced neuron model

Submitted: June 19, 2017; **Accepted:** August 7, 2017

1. Introduction

Previous study of spiking neuron models have shown that an applied magnetic field can affect their firing activity [1]. Results show that an external electric field has a significant impact on the performance of a neural network. A strong external electric field facilitates the firing of action potentials and enhances the mean firing rate of the neurons that comprise the network, but simultaneously, the synchronicity of network activity is disrupted. Yu *et al.* [2] investigated the effects of an induced electric field on a neural network and the result indicated that an inhibitory interneuronal network can only be synchronized within the range of gamma frequency (30–80 Hz). In this brief report, the properties of neural coding in spiking neural networks with biophysically reduced neurons in the presence of an exogenous alternating magnetic field are derived. Ebrahimian *et al.* [3] studies the parametric modeling of neurons under an extremely low frequency (50 Hz) sinusoidal environmental magnetic field. Electrophysiological recording from cells under current clamp were conducted to show the effects of magnetic fields on ion channels of the Hodgkin–Huxley cell model. Results indicated that low frequency magnetic fields with 50 Hz frequency directly lead to change in the bioelectric activities of neurons through a change in the amount and rate of open and closed ionic channels. The technique of magnetic stimulation has the potential to contribute to the study of the peripheral nervous system. Ruohonen *et al.* [4] discussed mathematical modeling of magnetic stimulation of the peripheral nerves. The work reveals recent theoretical advances, which may give new insight into the exact site of activation and help to understand the phenomena involved. Modolo *et al.* [5] studied the single neuron and neuronal network exposed to an extremely low frequency magnetic field. Results shed light on its effect on neuronal activity from the single cell to the network level, and illustrate the importance of a number of factors both in extremely low frequency magnetic field characteristics and brain tissue properties in determining the outcome of exposure. To provide insights into the modulation of neuronal activity by an extremely low frequency magnetic field, Yi *et al.* [6] presented a conductance-based neuronal model and introduced an extremely low frequency sinusoidal magnetic field as an additive voltage input. By analyzing spike times and spiking frequency, it was observed that neurons with distinct spiking patterns exhibited different response properties in the presence of magnetic field exposure. Camera *et al.* [7] performed simulations on neuronal models exposed to a specific pulsed magnetic field signal that seemed to be very effective in modulating the complex neuroelectromagnetic pulse. Results showed that such a pulse can silence the neurons of a feed-forward network for signal intensities that depend on the strength of the bias current and endogenous noise level. Jiang *et al.* [8] investigated the response of a two-dimensional neuronal model under an extremely low frequency magnetic field at different frequency and amplitude. By analyzing the shift in neuronal spike timing and average spiking frequency, it was found that the perturbation of neuronal spike timing and average spiking frequency induced by the magnetic field exposure was maximized for several harmonics of the intrinsic spiking frequency of the neuron. The study may contribute to guide future magnetic therapeutic developments.

2. Methods

The biophysically reduced model neuron of Izhikevich [9–11] was chosen as the deep spiking neural network unit; a deep spiking neural network based on synaptic plasticity was constructed; the firing rate and the interspike intervals (ISIs) of the spike sequence of the Izhikevich model neuron is close to the spiking firing properties of neurons and suited to large-scale simulation. The discrete time version of the Izhikevich model is given as:

$$
\begin{aligned}
v(t) &= v(t-1) + \Delta t(0.04v(t-1)^2 + \\
&\quad 5v(t-1) + 140 - u(t-1) + I), \\
u(t) &= u(t-1) + \Delta t a(bv(t-1) - u(t-1)), \\
&\text{if } v(t) \geq 30\text{mV, then } \begin{cases} v \leftarrow c; \\ u \leftarrow u + d; \end{cases}
\end{aligned} \tag{1}
$$

where $v(t)$ gives the membrane voltage of the model neuron, $u(t)$ is the recovery variable for membrane voltage, I gives the sum of external input current and synaptic currents, and Δt is the timestep. The Izhikevich neuron model can simulate a dozen different firing states of biological neurons by adjusting the dimensionless parameters a, b, c, d. The spiking pattern is used as the firing pattern of excitatory neurons in the neural network.Commonly used parameters are: $a = 0.02$; $b = 0.2$; $c = 65$; and $d = 8$, whereas, the low-threshold spiking pattern used to simulate the firing pattern of inhibitory interneurons in the network used: $a = 0.02$; $b = 0.25$; $c = -65$; $d = 2$.

2.1. The neuron model with applied magnetic field

Biologically, the extremely low frequency alternating magnetic field exerts effects on the firing sequence of a neuron through an induced electric field. According to the Faraday's law of electromagnetic induction, an alternating magnetic field produces an induced alternating electric field described by [2]:

$$
E(t) = \frac{r}{2}\frac{dB(t)}{dt} \tag{2}
$$

where r is the radius of the alternating magnetic field. A sinusoidal magnetic field generates an induced electric field with a cosine form.

The relationship between the external electric field E and the voltage ΔV can be described by [2]:

$$
\frac{d\Delta V}{dt} + \frac{\Delta V}{\tau} = \frac{\lambda}{\tau}E \tag{3}
$$

where τ is the Maxwell–Wagner time constant [12], and λ is the polarization length [13].

According to equations (2) and (3), when an alternating magnetic field is $B(t) = A\sin(2\pi ft)$, the voltage ΔV is given by [2]:

$$
\Delta V(t) = \pi rfA\lambda\frac{\cos(2\pi ft) + 2\pi f\tau\sin(2\pi ft)}{1 + (2\pi f\tau)^2} \tag{4}
$$

The magnitude of τ is generally 10^{-10} s and the frequency f is located in the range of the extremely low frequency, $2\pi f\tau \ll 1$. Therefore, the voltage ΔV is approximated as follows [2]:

$$
\Delta V(t) \approx \pi RfA\lambda\cos(2\pi ft). \tag{5}
$$

The voltage ΔV is an external voltage disturbance. The neuron membrane voltage $v(t)$ in the presence of an exogenous alternating magnetic field $B(t) = A\sin(2\pi ft)$ can be described as follows [14]:

$$
v(t) \rightarrow v(t) + \Delta V(t). \tag{6}
$$

The neuron model to be included in the spiking neural networks under the alternating magnetic field can be obtained by introducing equation (6) into the mathematical model of the Izhikevich quadratic model. The complexity of the Hodgkin–Huxley neuron model is high, so its simulation time of the Hodgkin–Huxley neuron model is too long for simulation of deep neural networks even with a supercomputer [15]. However, the Izhikevich neuron model gives qualitatively similar responses to the Hodgkin–Huxley neuron model and can simulate the firing behavior of real neurons. Therefore, the Izhikevich neuron model is suitable for simulating neuron discharge in large-scale deep neural networks. The answer as to whether super-computational neuroscience can facilitate implementation of Hodgkin–Huxley neuron models in deep neural networks remains to be seen [16].

2.2. Synaptic plasticity

When the j th post-synaptic neuron is not activated by the i th presynaptic neuron, the excitatory and inhibitory synaptic conductances depend on exponential decay, respectively:
Excitatory synapse:

$$
g_{ex}(t) = g_{ex}(t-1) - \Delta t(g_{ex}(t-1)/\tau_{ex}) \tag{7}
$$

Inhibitory synapse:

$$
g_{in}(t) = g_{in}(t-1) - \Delta t(g_{in}(t-1)/\tau_{in}). \tag{8}
$$

where $g_{ex}(t)$ is the excitatory synaptic conductance, $g_{in}(t)$ the inhibitory synaptic conductance, Δt is the differential step, τ_{ex} and τ_{in} respectively represent the decay constants of the excitatory and inhibitory conductances. In this study, $\tau_{ex} = \tau_{in} = 5$ ms.

When the jth postsynaptic neuron is activated by the ith presynaptic neuron, the excitatory and inhibitory synaptic conductances are given by:
Excitatory synapse:

$$
g_{ex}(t) = g_{ex}(t-1) + \bar{g}_{ex}(t), \tag{9}
$$

Inhibitory synapse:

$$
g_{in}(t) = g_{in}(t-1) + \bar{g}_{in}(t), \tag{10}
$$

where $\bar{g}_{ex}(t)$ and $\bar{g}_{in}(t)$ gives the increment of excitatory and inhibitory conductances, respectively. In the excitatory synapse model, $\bar{g}_{ex}(t) = \bar{g}_{ex}(t-1) + g_{\max}w_{i,j}(t)$; $w_{i,j}(t)$ is the synaptic modification function; $0 \leq \bar{g}_{ex}(t) \leq g_{\max}(g_{\max} = 0.015)$. When $\bar{g}_{ex}(t)$ is less than 0, $\bar{g}_{ex}(t)$ is set to 0; when $\bar{g}_{ex}(t)$ is larger than $g_{\max}$, $\bar{g}_{ex}(t)$ is set to $g_{\max}$. In the inhibitory synapse model, $\bar{g}_{in}(t)$ is set to 0.05.

2.3. A discrete time feed forward neural network

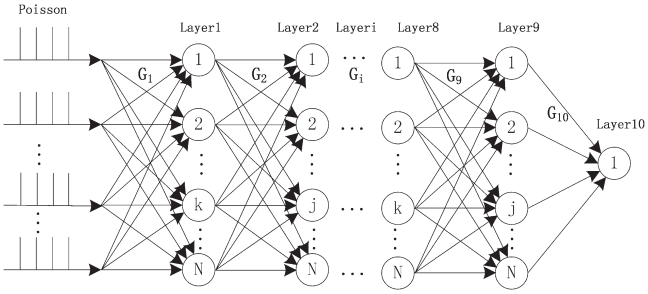

Fig. 1. Schematic illustration of the deep spiking feed forward neural network.Input to the deep spiking neural network is Poissonian. *Gi* is the synaptic conductance matrix of neurons in the *i*th layer in the deep spiking neural network, N is the number of neurons in each layer (except Layer 10), k and j give the pre- and post-synaptic neuron, respectively.

A deep spiking neural network with ten-layer feed forward topology is shown in Fig. 1. A oisson impulse distribution approximated the firing sequence of real neurons and was used as the input to the deep spiking neural network. Layers 1 to 9 each contained one hundred neurons. There was only one neuron in the output Layer 10. The ratio of excitatory neurons to inhibitory neurons was 4:1. When an afferent neuron was excitatory, the synapse contacting the postsynaptic neuron was excitatory, whereas, when the pre-synaptic neuron was inhibitory, the synapse onto the postsynaptic neuron was inhibitory. Thhere was no learning (retrograde information flow) in the simulated network [17]. The discrete timestep model of a deep spiking neural network was constructed as follows:

$$\begin{aligned} v_{i,j}(t) &= v_{i,j}(t-1)+\Delta t(0.04v_{i,j}^2(t-1)+5v_{i,j}(t-1)+140 \\ &\quad -u_{i,j}(t-1)+I_{ext}+I_{i,j}^{syn}(t)), \\ u_{i,j}(t) &= u_{i,j}(t-1)+\Delta ta(bv_{i,j}(t-1)-u_{i,j}(t-1)), \\ I_{i,j}^{syn}(t) &= \sum_{k=1}^{N} g_i(k,j,t)(E-v_{i,j}(t-1)), \\ G_i &= \{g_i(k,j,t)\,|\,i=1,2,3,\ldots,N_L; \\ &\quad k=j=1,2,3,\ldots,N; t=1,2,3,\ldots,T \end{aligned} \tag{11}$$

where $v_{i,j}(t)$ is the postsynaptic voltage of the j th neuron in the ith layer, $u_{i,j}(t)$ is the recovery variable of the j th neuron in the ith layer, Δt is the time step, I_{ext} is the external thalamic input, $I_{i,j}(t)$ is the sum of synaptic currents of the j th neuron in the ith layer, G_i is the synaptic conductance matrix of the neurons in the ith layer, $g_i(k,j,t)$ which is the synaptic conductance between presynaptic neuron k and postsynaptic neuron j in the ith layerwas regulated by the model of synaptic plasticity described in Section 2.2, N_L is the number of layers in the network, N is the number of neurons in each layer (excepting Layer 10), T is the simulation time, and E is the reversal potential. When the presynaptic neuron k is excitatory, E_{ex} was 0 mV when the presynaptic neuron k is inhibitory, $E_{in}(t)$ was 70 mV.

The parameter values for network initialization ($t=1$), were:

$$v_{i,j}(t=1)=-65\,\text{mV}; u_{i,j}(t=1)=bv_{i,j}(t=1); g_i(k,j,t=1)=0.015. \tag{12}$$

3. Results

Here, spiking neural network behavior was analyzed by using rate coding and temporal coding. Rate coding was employed as it one of the most widely reported neural information coding methods in neuroscience. Both current and traditional empirical results tend to be reported as rates [18–22]. The firing rate for a given temporal window is calculated as:

(1) Assuming t^n is the nth firing time of neuron i, the firing sequence H_i of neuron i can be described as follows:

$$H_i=\{\cdots t_i^n\cdots\}, t_i^1<t_i^2<\cdots<t_i^n<\cdots. \tag{13}$$

(2) Temporal window length is set to t_w. The firing rate γ_i of neuron i in the temporal window $[t-t_w,t]$ is then:

$$\gamma_i(t,t_w)=\frac{\eta_i(t-t_w,t)}{t_w} \tag{14}$$

Table 1. Mean firing rate under alternating magnetic field

Alternating magnetic field amplitude	Distribution range of the neuron mean firing rates	Mean firing rates of whole network
No magnetic field	5.20 ~ 9.99	8.67 ± 1.17
5 mT	5.41 ~ 10.00	8.72 ± 1.18
10 mT	5.41 ~ 10.83	9.01 ± 1.31
15 mT	5.62 ~ 11.88	9.64 ± 1.48
20 mT	5.62 ~ 10.84	9.66 ± 1.33
25 mT	5.83 ~ 12.50	10.19 ± 1.60

Where $\eta_i(\cdot)$ is the firing number of neuron i in the temporal window $[t-t_w,t]$. For this analysis the temporal window length t_w was 200 ms and the temporal window step size was 50 ms.

The range of magnetic field amplitude A was chosen to be 5 25 mT. When the amplitude A of the alternating magnetic field was 5 mT, 10 mT, 15 mT, 20 mT, 25 mT, the dynamic changes in mean firing rate of the deep spiking neural network are given in Fig. 2. The rate coding activity pattern of the neuron under the alternating magnetic field shows no change when compared with the condition of no magnetic field. With increased alternating magnetic field amplitude, the firing pattern of the neuron remains unchanged and firing synchronization becomes poor. Distribution range of the mean neuronal firing rates and the mean firing rate of the whole network under different alternating magnetic field amplitudes are given in Table 1.

From Table 1, the distribution range of mean firing rate of neuron expands with increased amplitude of the alternating magnetic field. The mean firing rate of the whole network is increased with increased amplitude of the alternating magnetic field. According to classical Hebbian coding theory, under the stimulation of an alternating magnetic field, the neurons whose firing rates increase simultaneously can beidentified as a functional neuron population to characterize the stimulation pattern of an alternating magnetic field.

The mean rate coding method can reflect the dynamic change of the mean firing rate. However, the real-time performance of the mean rate coding is poor since the firing rate of neurons obtained from a given temporal window is an average value. Alternatively, temporal coding shows the real-time evolution of interspike intervals of a spike train generated by a neural network. Thus, temporal coding is can be used to analyze the coding properties of spiking neural networks under alternating magnetic field stimulation.

Temporal coding relies on ISIs rather than statistical averaging to explore spike train timing. The pattern of the spike firing sequence is given by the intervals between spikes [23, 24]. Three types of descriptive methods ISI coding include the: ISI time domain diagram, ISI histogram, and joint ISI distribution. The ISI time domain diagram gives the distribution of ISIs and shows the dynamics of firing patterns in neural networks. The ISI histogram illustrates the overall distribution of ISIs. The joint ISI distribution can be used to identify specific recurrence patterns from the perspective of third-order coding. ISI time domain diagrams of a spiking neural network when the amplitude A of an alternating magnetic field stimulus is 5 mT, 10 mT, 15 mT, 20 mT, and 25 mT, are shown in Fig. 3.

Simulation results have shown that the temporal coding pattern of a neuron stimulated by an alternating magnetic field does not change compared with the condition where the alternating magnetic field is absent. With increased magnetic field amplitude, temporal

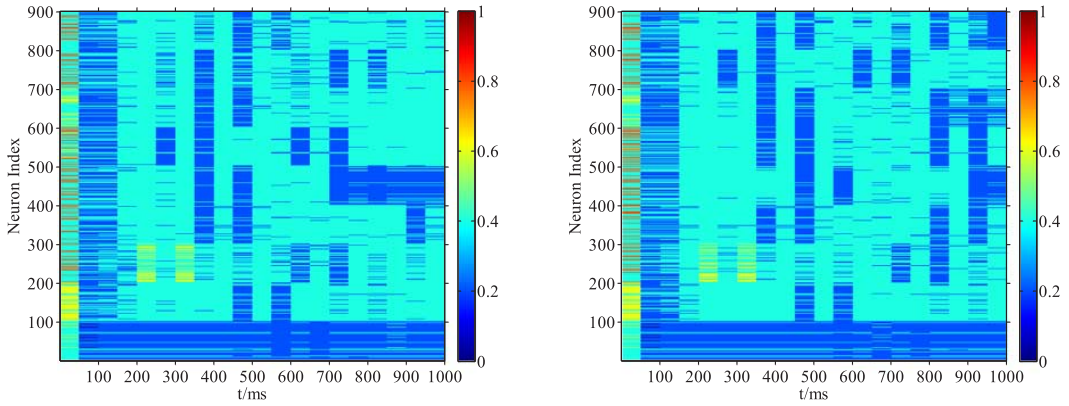

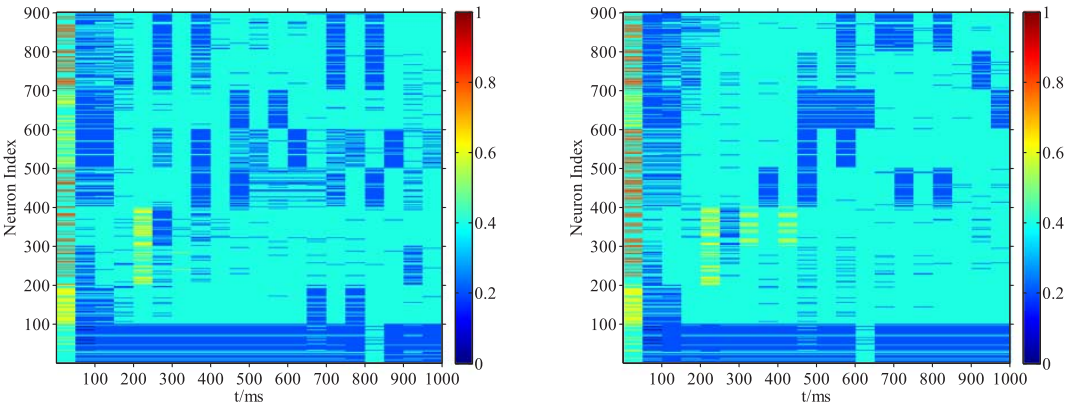

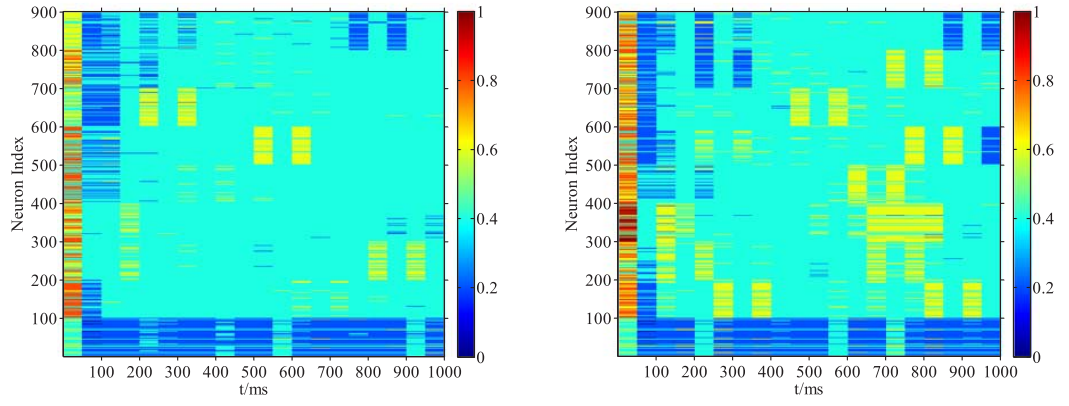

Fig. 2. Dynamic change of mean firing rate of the neuron under alternating magnetic field stimulation. Horizontal axis indicates simulation time and the vertical axis gives neuron index. Vertical color scale to the right ranges from red (high firing rate) to blue (low firing rate). a, the mean firing rate of the neurons in layer 1 is lower than the neurons in other layers, mean firing rate of neurons during the initial period is higher than other periods. b–f, under the alternating magnetic field, mean firing rate of neurons in layer 1 is also lower than the neurons in other layers; the mean firing rate of the neurons during the initial period is higher than other periods.

coding is enhanced. Correspondingly, the amplitude A of the alternating magnetic field is 5 mT, 10 mT, 15 mT, 20 mT, 25 mT, the distribution of ISI histograms of spiking neural network are shown in Fig. 4. Simulation results show that the distribution of the ISIs becomes uniform and ISIs become shorter under alternating magnetic field stimulation. Lower ISI values correspond to higher firing

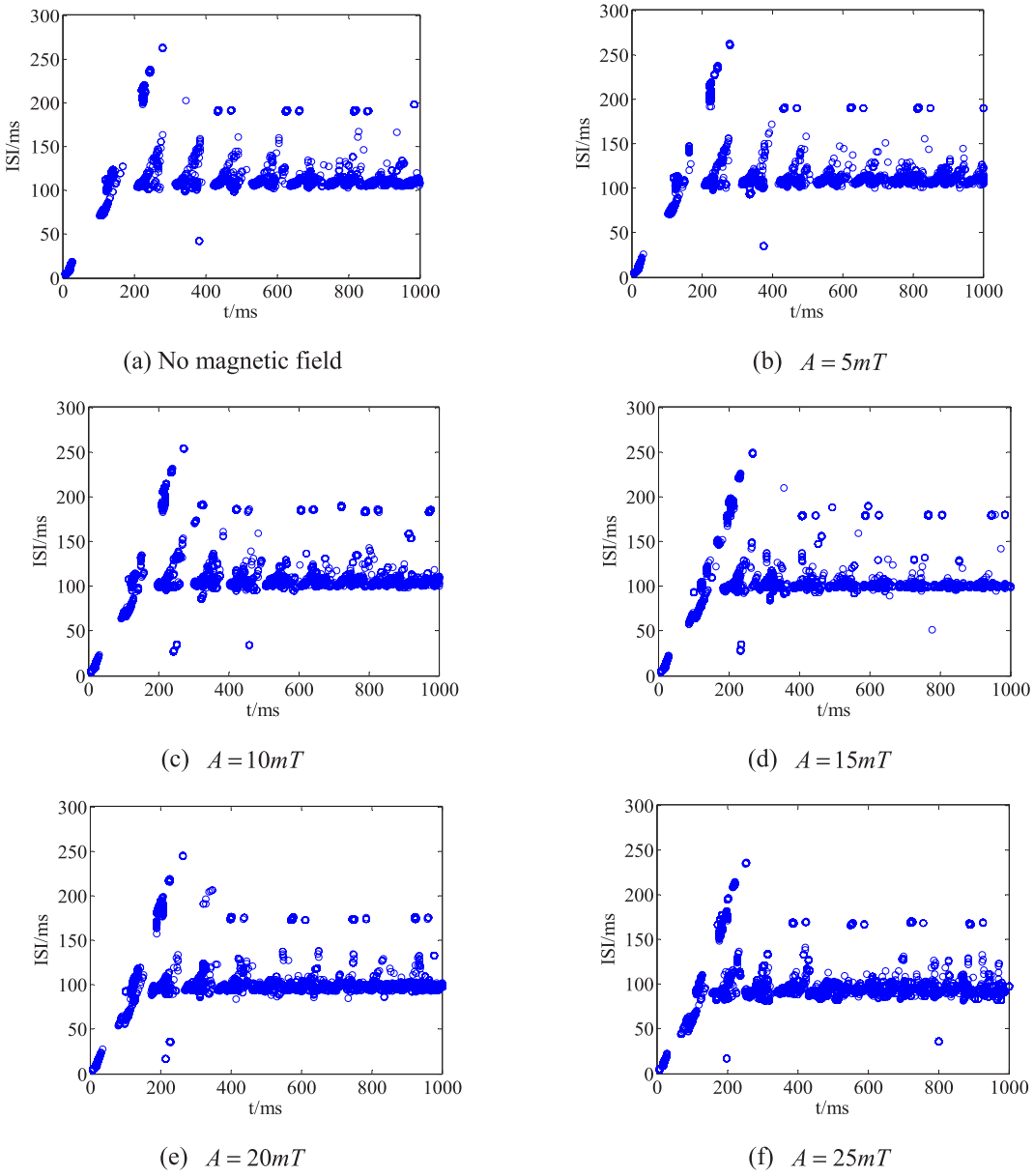

Fig. 3. ISI time domain diagram for a deep spiking neural network stimulated by an alternating magnetic field. Horizontal axis gives discrete time points of spike firing, vertical axis gives ISI value at spike firing time. For the 0–200 ms period the ISI distributionI was unstable and the distribution range of ISIs was 250 ms under the different amplitudes of the alternating magnetic field. During the period 200–1000 ms ISIs were divided into two populations in response to the different amplitudes of the alternating magnetic field. The top layer gives the ISIs between bursts of action potentials and ranges over 150–200 ms. The bottom layer gives ISIs inside the bursts of action potentials and ISIs range over 100–150 ms. Increased amplitude of the alternating magnetic field during the period 0–200 ms, decreases the ISI range, during the period from 200–1000 ms, the distribution range of the bottom layer ISIs is decreased.

rates. The ISI histogram indicates that an alternating magnetic field can increase the firing rate of a neural networke, which is consistent with the results of rate coding. Likewise, when the amplitude *A* of an alternating magnetic field is 5 mT, 10 mT, 15 mT, 20 mT, 25 mT, the joint ISI distributions of spiking neural network are shown in Fig. 5.

4. Conclusion

Based on a comprehensive analysis of ISI time domain diagrams, ISI histograms, and joint ISI distributions, the ISIs of the neurons in a spiking neural network are decreased and ISI distribution tends to be uniform under the stimulus of an alternating magnetic field. The firing rate is significantly increased under alternating magnetic field stimulation and the rate coded response is enhanced with increased stimulation intensity. The ISIs of the spiking sequence are decreased and the distribution of the ISIs tends be uniform under alternating magnetic field stimulation. Reduction of the spiking train ISIs generated by a spiking neural network corresponds to the higher firing rate so the temporal coding properties of spiking neural network under the alternating magnetic field become more consistent with rate coded properties.

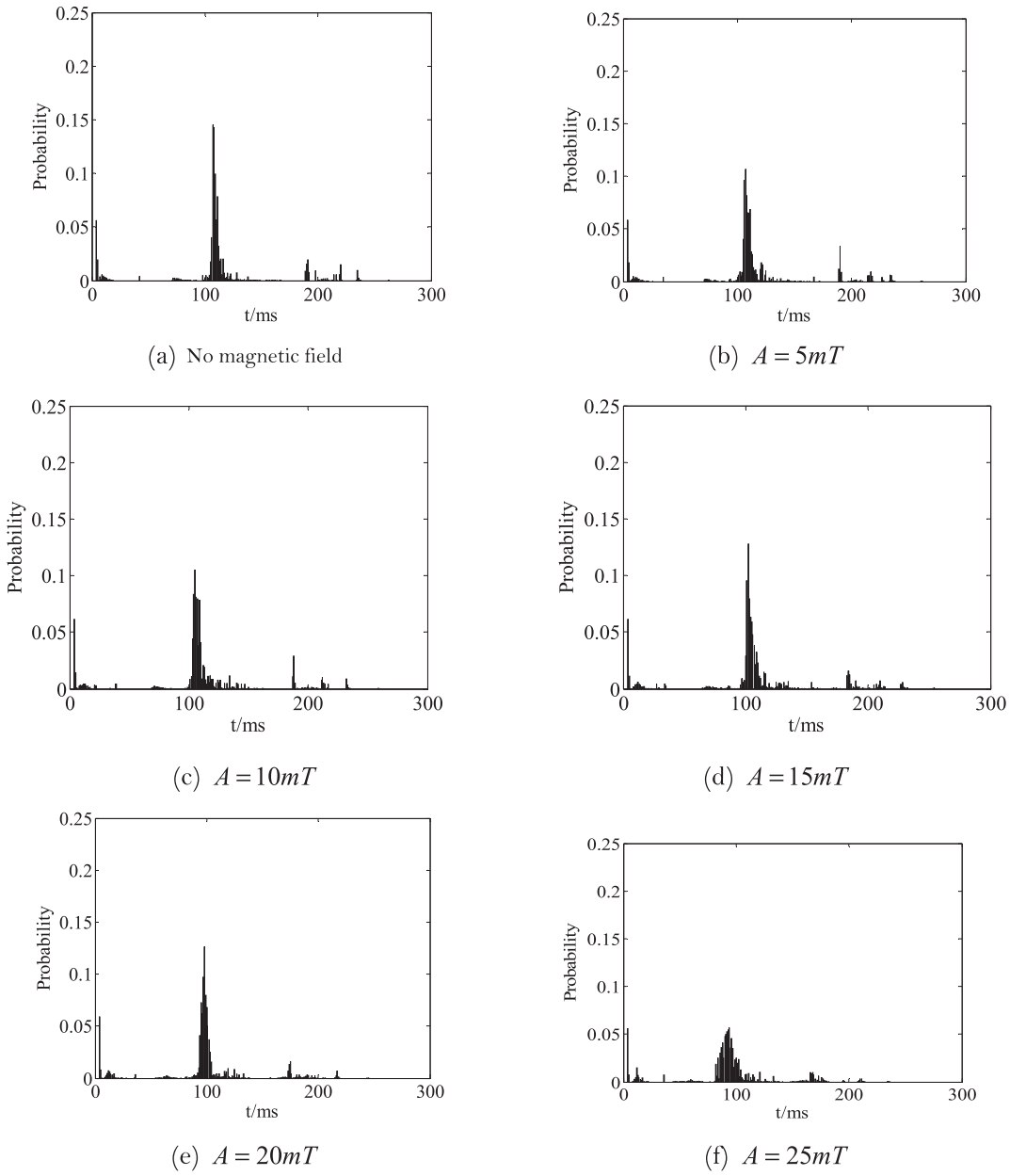

Fig. 4. ISI histogram obtained from a deep spiking neural network under alternating magnetic field stimulation. The horizontal axis gives different values of ISIs, vertical axis gives the repeated number of ISIs as a proportion of the total number of ISIs. a, the distribution of the ISIs is concentrated in a 100 ms period and the distribution of ISIs in the other period is less without stimulation. b–f, in the presence of an alternating magnetic field, the distribution of the ISIs is also concentrated within 100 ms. With increased amplitude of the alternating magnetic field, the distribution of ISIs in 100 ms is decreased and the distribution of ISIs in the other period is increased.

Acknowledgments

This work was supported by National Natural Science Foundation of China (No. 61571180, 31400844) and Natural Science Foundation of Hebei Province (No. E2016202128).

Conflict of Interest

All authors declare no conflicts of interest.

References

[1] Wang H, Chen Y (2016) Spatiotemporal activities of neural network exposed to external electric fields. *Nonlinear Dynamics* **85(2)**, 881-891.

[2] Kai Y, Jiang W, Deng B, Wei X (2013) Effects of Induced Electric Field on Network Synchrony Under Magnetic Stimulation. *Journal of Tianjin University* **46(8)**, 726-736.

[3] Ebrahimian H, Firoozabadi M, Janahmadi M (2013) Parametric modeling of nerve cell under the sinusoidal environmental 50 Hz extremely low frequency magnetic field. *Journal of Ardabil University of Medical Sciences* **13(2)**, 119-131.

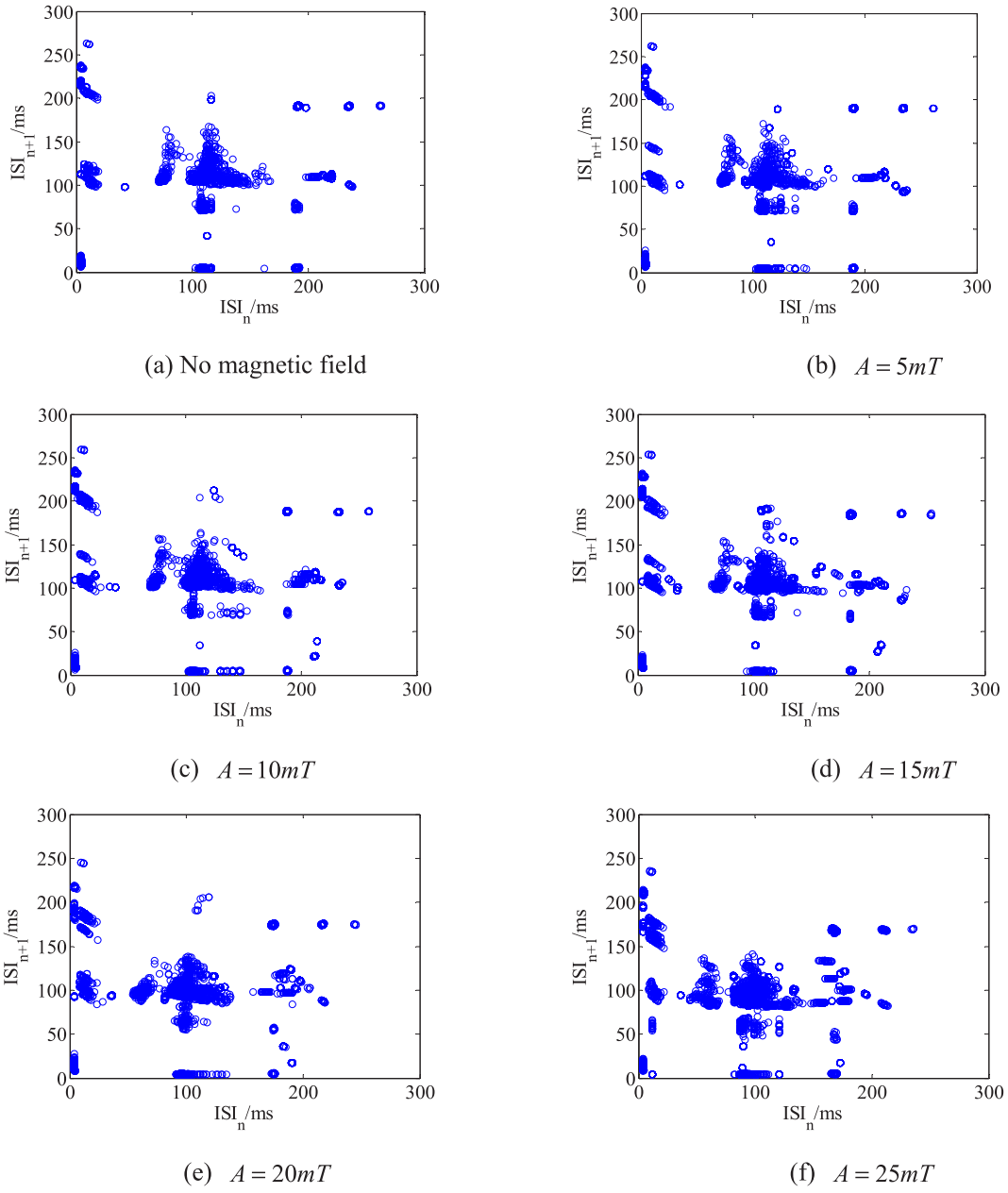

Fig. 5. Joint ISI distributions obtained from a spiking neural network under an alternating magnetic field stimulus. The horizontal axis gives each ISI(n) in the spike firing sequence; vertical axis gives adjacent ISI(n 1). a, in the absence of stimulation, most joint ISIs of neurons in the spiking neural network are distributed in the center and other joint ISIs are distributed along the horizontal and vertical axes. b–f, under an alternating magnetic field, the central coverage area of joint ISI distribution becomes dispersed and the distribution of the joint ISIs along the horizontal axis and vertical axes is increased. With increased amplitude of the alternating magnetic field, the distribution of the central coverage area of joint ISI becomes more dispersed.

[4] Ruohonen J, Ravazzani P, Tognola G, Grandori F (1997) Modeling peripheral nerve stimulation using magnetic fields. *Journal of the Peripheral Nervous System* **2(1)**, 17-29.

[5] Modolo J, Thomas AW, Stodilka RZ, Prato FS, Legros A (2010) Modulation of neuronal activity with extremely low-frequency magnetic fields: Insights from biophysical modeling. In, IEEE Fifth International Conference on Bio-Inspired Computing: Theories and Applications (pp. 1356-1364).

[6] Yi G, Wang J, Wei X, Deng B, Tsang KM, Chan WL, Han C (2014) Effects of extremely low-frequency magnetic fields on the response of a conductance-based neuron model. *International Journal of Neural Systems* **24(1)**, 527-584.

[7] Camera F, Thomas AW, Paffi A, D'Inzeo G, Apollonio F, Prato FS, Liberti M (2013) Effects of pulsed magnetic field on neurons: Cnp signal silences a feed-forward network model. In, International IEEE/EMBS Conference on Neural Engineering (pp. 223-226).

[8] Jiang XY, Wang J, Yi GS, Deng B, Wei XL, Han CX (2012) Effects of extremely low-frequency magnetic fields on neuron activity. In, Proceedings of the 31st Chinese Control Conference (pp. 7355-7359).

[9] Izhikevich EM (2004) Which model to use for cortical spiking neurons? *IEEE Transactions on Neural Networks* **15(5)**, 1063-1070.

[10] Izhikevich EM (2003) Simple model of spiking neurons. *IEEE Transactions on Neural Networks* **14(6)**, 1569-1572.

[11] Davey KR, Epstein CM, George MS, Bohning DE (2003) Modeling the effects of electrical conductivity of the head on the induced electric field in the brain during magnetic stimulation. *Clinical Neurophysiology* **114(11)**, 2204-2209.

[12] Bédard C, Kröger H, Destexhe A (2006) Model of low-pass filtering of local field potentials in brain tissue. *Physical Review E Statistical Nonlinear & Soft Matter Physics* **73(5 Pt 1)**, 051911.

[13] Radman T, Ramos RL, Brumberg JC, Bikson M (2009) Role of Cortical Cell Type and Morphology in Suband Suprathreshold Uniform Electric Field Stimulation. *Brain Stimulation* **2(4)**, 215-228, e213.

[14] Giann M, Liberti M, Apollonio F, Inzeo GD (2006) Modeling electromagnetic fields detectability in a HH-like neuronal system: stochastic resonance and window behavior. *Biological Cybernetics* **94(2)**, 118-127.

[15] Djurfeldt M, Lundqvist M, Johansson C, Rehn M, Ekeberg O, Lansner A (2008) Brain-scale simulation of the neocortex on the IBM Blue Gene/L supercomputer. *IBM Journal of Research & Development* **52(1, 2)**, 31-41.

[16] Graben PB, Zhou C, Thiel M, Kurths J (2008) Lectures in Supercomputational Neuroscience: Dynamics in Complex Brain Networks. *Journal of the Computational Structural Engineering Institute of Korea* **27(4)**, 297-303.

[17] Lecun Y, Bengio Y, Hinton G (2015) Deep learning. *Nature* **521(7553)**, 436-444.

[18] Paoli M, Weisz N, Antolini R, Haase A (2016) Spatially resolved time-frequency analysis of odour coding in the insect antennal lobe. *European Journal of Neuroscience* **44(6)**, 2387-2395.

[19] Won JH, Tremblay K, Clinard CG, Wright RA, Sagi E, Svirsky M (2016) The neural encoding of formant frequencies contributing to vowel identification in normal-hearing listeners. *Journal of the Acoustical Society of America* **139(1)**, 1-11.

[20] Jones HG, Brown AD, Koka K, Thornton JL, Tollin DJ (2015) Sound frequency-invariant neural coding of a frequency-dependent cue to sound source location. *Journal of Neurophysiology* **114(1)**, 531-539.

[21] Rosenbaum R, Zimnik A, Zheng F, Turner RS, Alzheimer C, Doiron B, Rubin JE (2014) Axonal and synaptic failure suppress the transfer of firing rate oscillations, synchrony and information during high frequency deep brain stimulation. *Neurobiology of Disease* **62(2)**, 86-99.

[22] Alvespinto A, Palmer AR, Lopezpoveda EA (2014) Perception and coding of high-frequency spectral notches: potential implications for sound localization. *Frontiers in Neuroscience* **8(8)**, 112.

[23] Tsubo Y, Isomura Y, Fukai T (2012) Power-Law Inter-Spike Interval Distributions Infer a Conditional Maximization of Entropy in Cortical Neurons. *Plos Computational Biology* **8(4)**, e1002461.

[24] Yang Y, Ramamurthy B, Neef A, Xu-Friedman MA (2016) Low Somatic Sodium Conductance Enhances Action Potential Precision in Time-Coding Auditory Neurons. *Journal of Neuroscience* **36(47)**, 11999-12009.